Turbulent diffusion in stably stratified non-decaying turbulence

By F. NICOLLEAU and J. C. VASSILICOS

Department of Applied Mathematics and Theoretical Physics, University of Cambridge,
Silver Street, Cambridge CB3 9EW, UK

We develop a Lagrangian model of both one-particle[†] and two-particle turbulent diffusion in high Reynolds number and low Froude number stably stratified non-decaying turbulence. This model is a kinematic simulation (KS) that obeys both the linearized Boussinesq equations and incompressibility. Hence, turbulent diffusion is anisotropic and is studied in all three directions concurrently with incompressibility satisfied at the level of each and every trajectory.

   Horizontal one-particle and two-particle diffusions are found to be independent of the buoyancy (Brünt–Väissälä) frequency N. For one-particle diffusion we find that

$$\langle (x_i(t) - x_i(t_0))^2 \rangle \sim u'^2(t - t_0)^2 \quad \text{for} \quad t - t_0 \ll L/u',$$

and

$$\langle (x_i(t) - x_i(t_0))^2 \rangle \sim u'L(t - t_0) \quad \text{for} \quad t - t_0 > L/u',$$

where $i = 1, 2$ and u' and L are a r.m.s. velocity and a length-scale of the energy-containing motions respectively, and

$$\langle (x_3(t) - x_3(t_0))^2 \rangle \simeq \frac{u'^2}{N^2} = L^2 Fr^2 \quad \text{for} \quad \frac{2\pi}{N} \ll t - t_0.$$

This capping of one-particle vertical diffusion requires the consideration of the entire three-dimensional flow, and we show that each and every trajectory is vertically bounded for all times if the Lagrangian vertical pressure acceleration a_3 is bounded for all times. Such an upper bound for a_3 can be derived from the linearized Boussinesq equations as a consequence of the coupling between vertical pressure acceleration and the horizontal and vertical velocities.

   Two-particle vertical diffusion exhibits two plateaux. The first plateau's scaling is different according to whether the initial separation Δ_0 between the two particles is larger or smaller than η, the smallest length-scale of the turbulence:

$$\left. \begin{array}{ll} \langle \Delta x_3^2 \rangle \simeq \Delta_0^2 Fr^2 (L/\eta)^{4/3} & \text{for} \quad \Delta_0 \leqslant \eta \\ \langle \Delta x_3^2 \rangle \simeq (\Delta_0/L)^{2/3} L^2 Fr^2 & \text{for} \quad \Delta_0 \geqslant \eta \end{array} \right\} \quad \text{for} \quad \frac{2\pi}{N} < t - t_0 < \frac{L}{u'}.$$

The second plateau is reached when the two particles become statistically independent, and therefore

$$\langle \Delta x_3^2 \rangle \simeq 2L^2 Fr^2 \quad \text{for} \quad t - t_0 \gg L/u'.$$

The transition between the two plateaux coincides with the time when the two particles start moving significantly apart in the horizontal plane.

---

† In this paper 'particle' and 'fluid element' are synonymous.

1. Introduction

Kinematic simulation (KS) is a unified Lagrangian model of one- and two- and in-deed multi-particle turbulent diffusion where incompressibility is enforced by construction in the generation of every particle trajectory, the energy spectrum is prescribed according to the type of turbulence considered and where the effects of small-scale flow structure on Lagrangian statistics are taken into account (Fung *et al.* 1992; Elliott & Majda 1996; Fung & Vassilicos 1998; Malik & Vassilicos 1999). As such, KS should be contrasted with Lagrangian stochastic models of turbulent diffusion which do not incorporate small-scale flow structure effects and which are by construction different models for one- and two-particle statistics. Stochastic models rely, at least in practice, on Wiener processes which are used to model Lagrangian velocities in one-particle models (van Dop, Nieuwstadt & Hunt 1985; Thomson 1987) and Lagrangian relative accelerations in two-particle models (see Pedrizzetti & Novikov 1994; Heppe 1997).

The small-scale geometry of one-particle trajectories does not affect their average and variance statistics because these statistics are to a great extent determined by the large energy-containing scales of the turbulence. However, as demonstrated by Fung *et al.* (1992), Fung & Vassilicos (1998) and Malik & Vassilicos (1999), two-particle statistics are very significantly influenced by small-scale spatio temporal flow structure, in particular eddying, straining and streaming regions (Perry & Chong 1987; Wray & Hunt 1990) and their time-dependence.

KS does not offer any particular advantage over other models of one-particle diffusion in the homogeneous isotropic case. However, the enforced incompressibility in KS, trajectory by trajectory, does mean that KS of non-isotropic turbulent flows can generate one-particle statistics in different directions in accordance with incompressibility. To our knowledge no Lagrangian model of one-particle turbulent diffusion to date has been developed to achieve such an objective. In this paper we develop a KS of stably stratified turbulence where one-particle diffusion can be studied concurrently under the constraint of incompressibility in all three directions, the direction of stratification and the plane normal to it.

As it is a unified model of both one- and two-particle turbulent diffusion, we also use the KS model of stably stratified turbulence to investigate two-particle statistics and the effect of small-scale turbulent flow structure on these statistics. The fundamental working hypothesis on which KS is based (Fung & Vassilicos 1998; Malik & Vassilicos 1999) is that a detailed and quantitatively precise modelling of the small-scale Eulerian flow structure is not required for an accurate determination of Lagrangian two-particle statistics, and that it is sufficient to incorporate in the KS model qualitatively correct incompressible Eulerian turbulent-like small-scale flow structure. The KS model is based on a kinematically simulated Eulerian velocity field which is generated as a sum of random incompressible Fourier modes. This velocity field incorporates turbulent-like flow structures, that is eddying, straining and streaming regions, in every realization of the Eulerian velocity field, and the Lagrangian model operates by integrating individual particle trajectories in many realizations of this velocity field. Thus, KS generates particle trajectories that are smooth and non-Markovian in a way directly determined by the turbulent-like incompressible Eulerian flow structures. Comparisons with direct numerical simulation results of two-particle statistics in stationary isotropic turbulence have shown good agreement with KS (Malik & Vassilicos 1999). Furthermore, the KS prediction for Richardson's constant G_Δ in three-dimensional isotropic homogeneous turbulence agrees well with Tatarski's (Tatarski 1960) experimental measurements (see Elliott & Majda 1996; Flohr & Vassilicos 2000).

In stratified turbulence, the stratification induces waves which interact with the turbulent velocity field and modify it. The effect of stratification on turbulent diffusion is therefore to modify the velocity field and thereby trap fluid elements and scalar concentrations in oscillatory motion. Turbulent diffusion in stably stratified turbulence has been studied with stochastic models (Csanady 1964; Pearson, Puttock & Hunt 1983; Heppe 1997), Direct numerical simulations (DNS) (Kimura & Herring 1996) and laboratory experiments (Britter *et al.* 1983). Stochastic models (Csanady 1964; Pearson *et al.* 1983; Heppe 1997) predict a vanishing vertical turbulent diffusivity in both decaying and non-decaying stably stratified turbulence, and the evidence from both DNS (Kimura & Herring 1996) and laboratory experiments (Britter *et al.* 1983) is that a régime and a range of time scales indeed exist where there is no vertical diffusion in stably stratified *decaying* turbulence. However no such evidence is currently available for stably stratified *non-decaying* turbulence. Laboratory experiments and DNS of forced stably stratified turbulence are difficult to perform and in fact DNS is also quite severely limited in Reynolds numbers and integration time.

The predictions of stochastic models for high Reynolds number non-decaying stably stratified turbulence need to be discussed in comparison with predictions of other models. Indeed stochastic modelling is based on the assumption that the pressure force in the Navier–Stokes equation is effectively random and delta-correlated in time in the limit of infinite Reynolds numbers. Furthermore, these stochastic models are one-dimensional and do not enforce incompressibility on every trajectory. The purpose of the present paper is to use KS for stably stratified *non-decaying* turbulence to investigate turbulent diffusion in the vertical and horizontal directions concurrently under the constraint of incompressibility and in the limit of high Reynolds numbers without direct assumptions on the pressure force. Following the stochastic modelling of Csanady (1964), Pearson *et al.* (1983) and Heppe (1997) and the DNS of Kimura & Herring (1996) our KS is based on the Boussinesq equations.

2. Lagrangian Boussinesq equations

Given a stably stratified fluid at static equilibrium, with pressure $p(x_3)$ and density $\rho(x_3)$ varying only in the direction x_3 of stratification such that $\mathrm{d}p/\mathrm{d}x_3 = -\rho g$ where $\boldsymbol{g} = (0, 0, -g)$ is the gravitational acceleration vector and $\boldsymbol{x} = (x_1, x_2, x_3)$, the Boussinesq equations determine perturbations around this equilibrium. Assuming the perturbation velocity field $\boldsymbol{u}(\boldsymbol{x}, t) = (u_1, u_2, u_3)$ to be incompressible, and the perturbation density $\rho'(\boldsymbol{x}, t)$ to be much smaller than ρ ($\rho' \ll \rho$) and denoting the perturbation pressure field by p', these equations are

$$\frac{\mathrm{D}}{\mathrm{D}t} \frac{\rho'}{\rho} = -u_3 \frac{1}{\rho} \frac{\mathrm{d}\rho}{\mathrm{d}x_3}, \tag{2.1}$$

$$\frac{\mathrm{D}}{\mathrm{D}t} \boldsymbol{u} = -\frac{1}{\rho} \nabla p' + \frac{\rho'}{\rho} \boldsymbol{g}, \tag{2.2}$$

$$\nabla \cdot \boldsymbol{u} = 0, \tag{2.3}$$

where we have omitted terms describing molecular diffusion and viscosity and $\mathrm{D}/\mathrm{D}t = \partial/\partial t + \boldsymbol{u} \cdot \nabla$. Even though strictly speaking, ρ is a function of x_3, in the Boussinesq approximation one considers a layer of stratified fluid of vertical extent small enough for ρ and $\partial\rho/\partial x_3$ to be effectively independent of x_3 within the layer, and the thickness of this layer can be estimated as being much smaller than $H = \rho/|\mathrm{d}\rho/\mathrm{d}x_3|$ (stable stratification requires $\mathrm{d}\rho/\mathrm{d}x_3 < 0$). Setting $\Theta = \rho'/\rho$ and $\boldsymbol{a} = (a_1, a_2, a_3) = -(1/\rho)\nabla p'$,

the Lagrangian Boussinesq equations for the Lagrangian coordinates $x_1(t)$, $x_2(t)$, $x_3(t)$ of fluid particles are

$$\ddot{x}_1(t) = a_1(t), \tag{2.4}$$

$$\ddot{x}_2(t) = a_2(t), \tag{2.5}$$

$$\ddot{x}_3(t) = a_3(t) - \Theta(t)g, \tag{2.6}$$

$$\dot{\Theta}(t) = \frac{u_3(t)}{H}, \tag{2.7}$$

where $\Theta(t)$ and $u_3(t)$ are the values of Θ and u_3 at the points visited by fluid element trajectories at time t. From (2.6) and (2.7) we obtain the following Lagrangian Boussinesq equation for vertical diffusion:

$$\ddot{x}_3 = a_3 - N^2(x_3 - x_3(t_0)) - g\Theta(t_0) \tag{2.8}$$

where $N^2 = g/H = g|\mathrm{d}\rho/\mathrm{d}x_3|/\rho$ and t_0 is the time of release.

In the absence of pressure acceleration a_3, fluid elements simply oscillate around $x_3(t_0) - (g/N^2)\Theta(t_0)$ with the buoyancy (Brünt–Väissälä) frequency N which is characteristic of stable stratification. Stochastic models of vertical diffusion in turbulent stably stratified flows (Csanady 1964; Pearson *et al.* 1983; Heppe 1997; Kimura & Herring 1996) start from the assumption that the vertical pressure acceleration is effectively a random acceleration delta-correlated in time. One consequence of this assumption is the decoupling of vertical and horizontal diffusion from the outset. However the incompressibility requirement (2.3) imposes a coupling between vertical and horizontal displacements and a dependence of the vertical pressure acceleration on both. Indeed, the incompressibility requirement (2.3) applied to (2.2) implies that

$$\nabla^2 p' = -\rho g \frac{\partial \Theta}{\partial x_3} - \rho \frac{\partial}{\partial x_i} u_j \frac{\partial}{\partial x_j} u_i \tag{2.9}$$

with a summation over i, j. This Poisson equation is readily solved by Fourier transformation leading to

$$\frac{1}{\rho}\frac{\partial}{\partial x_3}p' = -g \int \mathrm{d}\boldsymbol{k} \, \mathrm{e}^{\mathrm{i}\boldsymbol{k}\cdot\boldsymbol{x}} \frac{k_3^2}{k^2} \tilde{\Theta}(\boldsymbol{k},t)$$

$$+ \mathrm{i} \int \mathrm{d}\boldsymbol{k} \, \mathrm{e}^{\mathrm{i}\boldsymbol{k}\cdot\boldsymbol{x}} \frac{k_3}{k^2} \int \mathrm{d}\boldsymbol{k}' k_i'(k_j - k_j') \tilde{u}_j(\boldsymbol{k}',t) \tilde{u}(\boldsymbol{k}-\boldsymbol{k}',t) \tag{2.10}$$

where $\tilde{\Theta}(\boldsymbol{k},t)$ and $\tilde{u}_i(\boldsymbol{k},t)$ are the Fourier transforms of $\Theta(\boldsymbol{x},t)$ and $u_i(\boldsymbol{x},t)$ respectively with wavenumber $\boldsymbol{k} = (k_1,k_2,k_3)$ and $k^2 = \boldsymbol{k}\cdot\boldsymbol{k}$. The Lagrangian vertical pressure acceleration $a_3(t)$ is therefore given by

$$a_3(t) = g \int \mathrm{d}\boldsymbol{k} \, \mathrm{e}^{\mathrm{i}\boldsymbol{k}\cdot\boldsymbol{x}(t)} \frac{k_3^2}{k^2} \tilde{\Theta}(\boldsymbol{k},t)$$

$$- \mathrm{i} \int \mathrm{d}\boldsymbol{k} \, \mathrm{e}^{\mathrm{i}\boldsymbol{k}\cdot\boldsymbol{x}(t)} \frac{k_3}{k^2} \int \mathrm{d}\boldsymbol{k}' k_i'(k_j - k_j') \tilde{u}_j(\boldsymbol{k}',t) \tilde{u}(\boldsymbol{k}-\boldsymbol{k}',t) \tag{2.11}$$

where the dependence on the Lagrangian trajectory $\boldsymbol{x}(t)$ is manifest for all directions vertical and horizontal.

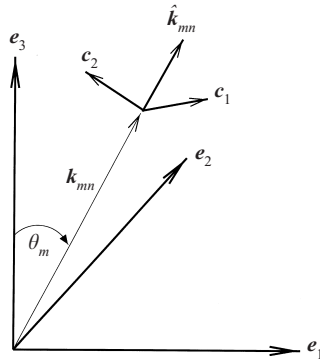FIGURE 1. The wavevector k_{mn} and the Craya–Herring frame c_1, c_2, $\hat{k}_{mn} = k_{mn}/k_n$ which is orthonormal. The frame e_1, e_2, e_3 is also orthonormal, e_1, e_2 are horizontal and e_3 vertical and θ_n is the angle between e_3 and k_{mn}.

Rather than make an assumption about a_3 and artificially decouple horizontal from vertical displacements, with KS one directly models the three-dimensional Eulerian velocity field $u(x, t)$ in accordance with certain turbulence statistics and physical requirements and solves $\dot{x}(t) = u(x(t), t)$. Hence KS can in particular be used to investigate the consistency of assumptions on a_3 with incompressible turbulent-like velocity fields. We now detail how and the régime for which we model the Eulerian velocity field $u(x(t), t)$ of a stably stratified velocity field.

3. Linearized Eulerian Boussinesq equations

Consider an initial velocity field $u(x, 0)$ with spatial fluctuations over a wide range of length scales, the smallest of these length scales being η. In the limit where the microscale Froude number is much smaller than 1, i.e. $Fr_\eta \equiv u(\eta)/N\eta \ll 1$ where $u(\eta)$ is the characteristic initial velocity fluctuation at that scale, and in the case where $u(\eta)$ corresponds to the smallest characteristic time scale in the initial flow, the Eulerian Boussinesq equations (2.1) and (2.2) may be approximated by their linear counterparts

$$\frac{\partial}{\partial t}\Theta = -u_3 \frac{1}{\rho}\frac{\mathrm{d}}{\mathrm{d}x_3}\rho, \tag{3.1}$$

$$\frac{\partial}{\partial t}u = -\frac{1}{\rho}\nabla p' + \Theta g \tag{3.2}$$

(see Hanazaki & Hunt 1996). Of course, the small Froude number limit cannot guarantee that (3.2) is a good approximation for the horizontal components of u. In the horizontal plane the linear approximation (3.2) may be expected to hold for times t smaller than an integral time scale L/u' where L is a length scale characteristic of the energy-containing motions of the turbulence and u' a r.m.s. velocity.

We use the Fourier transform $\tilde{u}(k, t)$ of $u(x, t)$ to solve equations (3.1) and (3.2) so that the incompressibility constraint (2.3) is transformed into $k \cdot \tilde{u}(k, t) = 0$ whilst the pressure field gradient is transformed into a vector parallel to k in Fourier space. Letting e_3 be the unit vector in the direction of stratification and e_1, e_2 two unit vectors normal to each other and to e_3 (so that $x = x_1e_1 + x_2e_2 + x_3e_3$ and $g = -ge_3$), the Craya–Herring frame (see figure 1) is given by the unit vector $\hat{k} = k/k$ and $c_1 = e_3 \times k/|e_3 \times k|$, $c_2 = k \times c_1/|k \times c_1|$. In the Craya–Herring frame the Fourier

transformed velocity field $\tilde{\boldsymbol{u}}(\boldsymbol{k}, t)$ lies in the plane defined by $\boldsymbol{c}_1$ and $\boldsymbol{c}_2$, i.e.

$$\tilde{\boldsymbol{u}}(\boldsymbol{k}, t) = \tilde{v}_1(\boldsymbol{k}, t)\boldsymbol{c}_1 + \tilde{v}_2(\boldsymbol{k}, t)\boldsymbol{c}_2, \qquad (3.3)$$

and is therefore decoupled from the pressure fluctuations which are along $\boldsymbol{k}$. Incompressible solutions of equations (3.1) and (3.2) in Fourier space and in the Craya–Herring frame are (Godeferd & Cambon 1994)

$$\tilde{v}_1(\boldsymbol{k}, t) = \tilde{v}_1(\boldsymbol{k}, 0), \qquad (3.4)$$

$$\tilde{v}_2(\boldsymbol{k}, t) = \tilde{v}_2(\boldsymbol{k}, 0) \cos{(Nt \sin\theta)}, \qquad (3.5)$$

$$\tilde{\Theta}(\boldsymbol{k}, t) = \frac{N}{g} \tilde{v}_2(\boldsymbol{k}, 0) \sin{(Nt \sin\theta)}, \qquad (3.6)$$

where $\theta = \theta(\boldsymbol{k})$ is the angle between $\boldsymbol{k}$ and $\boldsymbol{e}_3$ and the initial conditions are $\tilde{v}_1(\boldsymbol{k}, 0)$, $\tilde{v}_2(\boldsymbol{k}, 0)$ and $\tilde{\Theta}(\boldsymbol{k}, 0) = 0$ (zero initial potential). Because $u(\eta)$ corresponds to the smallest time scale in the turbulence, the condition $Fr_\eta \ll 1$ which is required for the linear solutions (3.4), (3.5), (3.6) to approximate the incompressible solution of the full nonlinear equations (2.1)–(2.2) implies

$$Fr = \frac{u'}{NL} \ll \frac{\eta}{u(\eta)} \bigg/ \frac{L}{u'}$$

where L is a length scale characteristic of the energy-containing motions of the turbulence and u' a r.m.s. velocity (Hanazaki & Hunt 1996). Note that the ratio of inner to outer time scales $(\eta/u(\eta))/(L/u')$ decreases as the Reynolds number increases. Hence the linearized Eulerian Boussinesq equations are valid for smaller and smaller Froude numbers as the Reynolds numbers is made larger and larger. Also, strictly speaking, L should be smaller than H and the time t smaller than L/u'.

We now introduce the KS model of the turbulence with which we specify the initial conditions $\tilde{v}_1(\boldsymbol{k}, 0)$ and $\tilde{v}_2(\boldsymbol{k}, 0)$ so that (3.4), (3.5), (3.6) represent the linear distortion of the turbulence by the stratification. In this model the Lagrangian vertical pressure acceleration $a_3(t)$ is determined by the linear part of (2.11), i.e.

$$a_3(t) = g \int \mathrm{d}\boldsymbol{k} \, \mathrm{e}^{\mathrm{i}\boldsymbol{k}\cdot\boldsymbol{x}(t)} \frac{k_3^2}{k^2} \tilde{\Theta}(\boldsymbol{k}, t) = N \int \mathrm{d}\boldsymbol{k} \, \mathrm{e}^{\mathrm{i}\boldsymbol{k}\cdot\boldsymbol{x}(t)} \frac{k_3^2}{k^2} \tilde{v}_2(\boldsymbol{k}, 0) \sin{(Nt \sin\theta)} \qquad (3.7)$$

where use is made of (3.6).

4. The KS Eulerian velocity field

The initial three-dimensional velocity perturbation to the stably stratified equilibrium is taken to be incompressible, isotropic and with a $-\frac{5}{3}$ large-wavenumber energy spectrum. (Some observational support for a $-\frac{5}{3}$ energy spectrum in the ocean has been obtained at depths where the Froude number is much smaller than one (see Gargett *et al.* 1984).) The Eulerian velocity field synthesized for homogeneous and isotropic three-dimensional KS is indeed such a field and we now use it to model these initial turbulent velocity fluctuations. Starting from the Fourier representation

$$\begin{aligned}
\boldsymbol{u}(\boldsymbol{x}, 0) &= \int_{-\infty}^{\infty} \int_{-\infty}^{\infty} \int_{-\infty}^{\infty} \tilde{\boldsymbol{u}}(\boldsymbol{k}, 0) \, \mathrm{e}^{\mathrm{i}\boldsymbol{k}\cdot\boldsymbol{x}} \, \mathrm{d}\boldsymbol{k} \\
&= \int_{-\infty}^{\infty} \int_{-\infty}^{\infty} \int_{-\infty}^{\infty} [\tilde{v}_1(\boldsymbol{k}, 0)\boldsymbol{c}_1(\boldsymbol{k}) + \tilde{v}_2(\boldsymbol{k}, 0)\boldsymbol{c}_2(\boldsymbol{k})] \, \mathrm{e}^{\mathrm{i}\boldsymbol{k}\cdot\boldsymbol{x}} \, \mathrm{d}\boldsymbol{k},
\end{aligned} \qquad (4.1)$$

where $\tilde{v}_1^*(\boldsymbol{k}, 0) = -\tilde{v}_1(-\boldsymbol{k}, 0)$ and $\tilde{v}_2^*(\boldsymbol{k}, 0) = -\tilde{v}_2(-\boldsymbol{k}, 0)$, the KS velocity field is constructed by discretizing (4.1), i.e

$$\boldsymbol{u}(\boldsymbol{x}, 0) = \sum_{n=1}^{N_k} \sum_{m=1}^{M_\theta} \sum_{j=1}^{J_\phi} k_n^2 \sin\theta_m \Delta k_n \Delta\theta_m \Delta\phi_j \, \mathrm{e}^{\mathrm{i}\boldsymbol{k}_{mnj}\cdot\boldsymbol{x}}$$
$$\times [\tilde{v}_1(\boldsymbol{k}_{mnj}, 0)\boldsymbol{c}_1(\boldsymbol{k}_{mnj}) + \tilde{v}_2(\boldsymbol{k}_{mnj}, 0)\boldsymbol{c}_2(\boldsymbol{k}_{mnj})], \quad (4.2)$$

with obvious notation and $\boldsymbol{k}_{mnj} = k_n(\sin\theta_m \cos\phi_j, \sin\theta_m \sin\phi_j, \cos\theta_m)$. Note that $\boldsymbol{u}(\boldsymbol{x}, 0)$ is three-dimensional and incompressible by construction because it is appropriately cast in the Craya–Herring representation. The directions and orientations of $\boldsymbol{k}_{\mathrm{mnj}}$ are chosen randomly for isotropy (see Fung *et al.* 1992; Malik & Vassilicos 1999). In this particular study, we take $\theta_m = (m-1)\pi/(M_\theta - 1)$ and $M_\theta = 20$ and for each pair n, m we randomly pick out one ϕ_j between 0 and 2π and $\phi_j + \pi$, i.e. $J_\phi = 2$ and $\Delta\phi_j = \pi$, and the notation ϕ_j should be replaced by ϕ_{nm}. Hence,

$$\boldsymbol{u}(\boldsymbol{x}, 0) = 2\pi \,\mathrm{Re} \left\{ \sum_{n=1}^{N_k} \sum_{m=1}^{M_\theta} k_n^2 \sin\theta_m \Delta k_n \Delta\theta_m \mathrm{e}^{\mathrm{i}\boldsymbol{k}_{mn}\cdot\boldsymbol{x}} \right.$$
$$\left. \times [\tilde{v}_1(\boldsymbol{k}_{mn}, 0)\boldsymbol{c}_1(\boldsymbol{k}_{mn}) + \tilde{v}_2(\boldsymbol{k}_{mn}, 0)\boldsymbol{c}_2(\boldsymbol{k}_{mn})] \right\} \quad (4.3)$$

where $\boldsymbol{k}_{\mathrm{mn}} = k_n(\sin\theta_m \cos\phi_{nm}, \sin\theta_m \sin\phi_{nm}, \cos\theta_m)$ (see figure 1) and Re stands for real part. The choice of discretized wavenumbers is made with reference to the energy spectrum $E(k)$ which is chosen such that

$$E(k) = E_0 L_0 \, (kL_0)^{-5/3} \quad (4.4)$$

for $k \geqslant L_0^{-1}$ and

$$E(k) = E_0 L_0 \, (kL_0)^4 \quad (4.5)$$

for $k \leqslant L_0^{-1}$, L_0^{-1} being the energy-containing scale where the energy spectrum takes its maximum value and E_0 is a characteristic energy of the energy-containing eddies at L_0^{-1}. As observed by Malik & Vassilicos (1999), the detailed modelling of the dissipation range has no impact on two-particle statistics even at short times, and we simply introduce a sharp viscous cutoff to this spectrum by setting

$$E(k) = 0 \quad (4.6)$$

for $k \geqslant k_{max} = 2\pi/\eta$ and we chose

$$k_n = k_{min} \left(\frac{k_{max}}{k_{min}} \right)^{(n-1)/N_k - 1} \quad \text{and} \quad k_{min} = \frac{1}{4L_0}.$$

In this study $N_k = 50$, except in figures 3 and 4 where $N_k = 1000$ (but the results plotted in figures 3 and 4 are effectively the same when $N_k = 50$). To ensure that the energy spectrum of the velocity field (4.3), and more generally (4.2), is given by (4.4), (4.5) and (4.6) we determine the amplitudes of $\tilde{v}_1(\boldsymbol{k}, 0)$ and $\tilde{v}_2(\boldsymbol{k}, 0)$ by

$$2|\tilde{v}_1(\boldsymbol{k}, 0)|^2 = |\tilde{v}_2(\boldsymbol{k}, 0)|^2 = \frac{2}{3} \frac{E(k)}{k^4 \Delta k} \quad (4.7)$$

(see Fung *et al.* 1992; Malik & Vassilicos 1999), and the phases of $\tilde{v}_1(\boldsymbol{k}, 0)$ and $\tilde{v}_2(\boldsymbol{k}, 0)$ are chosen randomly to enforce isotropy of the initial perturbation field.

We use the following definitions of u' and L, a r.m.s. velocity and integral length

scale (longitudinal) of the initial isotropic turbulence:

$$u'^2 = \frac{1}{2} \int E(k)\,\mathrm{d}k, \quad L = \frac{3\pi}{4} \frac{\int k^{-1} E(k)\,\mathrm{d}k}{\int E(k)\,\mathrm{d}k}.$$

5. The KS model of turbulent diffusion in high Reynolds number and low Froude number stratified non-decaying turbulence

KS is a Lagrangian model of turbulent diffusion and should therefore be evaluated on the basis of the Lagrangian statistics it generates. The present KS model of turbulent diffusion in stratified non-decaying turbulence consists of solving

$$\dot{\boldsymbol{x}}(t) = \boldsymbol{u}(\boldsymbol{x}(t), t) \tag{5.1}$$

to obtain a statistical ensemble of Lagrangian trajectories $\boldsymbol{x}(t)$ in a velocity field

$$\boldsymbol{u}(\boldsymbol{x}, t) = 2\pi\, \mathrm{Re}\left\{ \sum_{n=1}^{N_k} \sum_{m=1}^{M_\theta} k_n^2 \sin\theta_m \Delta k_n \Delta\theta_m \mathrm{e}^{\mathrm{i}\boldsymbol{k}_{\mathrm{mn}}\cdot\boldsymbol{x}} \right.$$
$$\left. \times\, [\tilde{v}_1(\boldsymbol{k}_{mn}, t)\boldsymbol{c}_1(\boldsymbol{k}_{mn}) + \tilde{v}_2(\boldsymbol{k}_{mn}, t)\boldsymbol{c}_2(\boldsymbol{k}_{mn})] \right\} \tag{5.2}$$

where

$$\tilde{v}_1(\boldsymbol{k}_{mn}, t) = \tilde{v}_1(\boldsymbol{k}_{mn}, 0), \tag{5.3}$$
$$\tilde{v}_2(\boldsymbol{k}_{mn}, t) = \tilde{v}_2(\boldsymbol{k}_{mn}, 0) \cos(Nt \sin\theta_m), \tag{5.4}$$

and $\tilde{v}_1(\boldsymbol{k}_{mn}, 0)$, $\tilde{v}_2(\boldsymbol{k}_{mn}, 0)$ are specified in §4 in accordance with an energy spectrum that has a $-\frac{5}{3}$ large-wavenumber scaling. This velocity field is not isotropic and results from the linear Boussinesq distortion (3.4) and (3.5) applied to the initially isotropic velocity field (4.3).

At this stage it is important to state that this KS model is a finite Reynolds number model in spite of the fact that (5.3) and (5.4) are obtained from solving the non-dissipative linear Boussinesq equations (3.1) and (3.2). Indeed, we have not included viscous forces in the Boussinesq equations but we have set a large-wavenumber cutoff $k_{max} = 2\pi/\eta$ for the initial turbulent velocity field's energy spectrum which we mean to represent the equilibrium viscous dissipation scale of the non-decaying turbulence. Hence, we incorporate viscous effects in the initial turbulent velocity perturbation field but not in the linear Boussinesq equations which we only use to calculate the linear distortion of this field by the density stratification. This approximation is appropriate for linearly distorted non-decaying turbulence and is valid in the double limit of large but finite Reynolds numbers Re (viscous forces small compared to inertial forces) and small Froude numbers (inertial forces small compared to buoyancy forces). In accordance with Kolmogorov's equilibrium theory we may expect that $Re \sim (L/\eta)^{4/3}$, and in this paper the ratio of the outer to the inner length scale L/η of the scale-invariant range varies between 4 and 24 (Lk_{max} varies between 26 and 146). Even though we can specify the ratio L/η we cannot give a value for the corresponding Reynolds number because we do not know the coefficient linking Re to $(L/\eta)^{4/3}$.

We start by computing $\overline{u_1^2}$, $\overline{u_2^2}$ and $\overline{u_3^2}$ as functions of time (see figure 2) where the overbars denote an average over 20 positions $\boldsymbol{x}$ taken from 40 realizations of the flow.
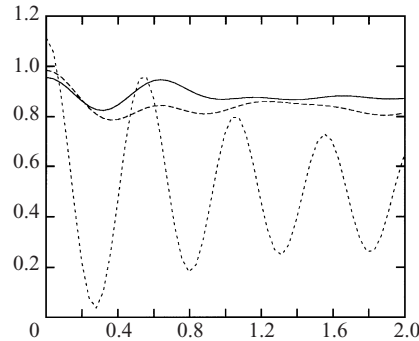
FIGURE 2. Eulerian velocity variance as function of time. From isotropy to anisotropy: continuous line $\overline{u_1^2}(t)/\frac{2}{3}u'^2$, dashed line $\overline{u_2^2}(t)/\frac{2}{3}u'^2$, dotted line $\overline{u_3^2}(t)/\frac{2}{3}u'^2$, as functions of $tN/2\pi$; $Fr = 0.0085$, $Lk_{max} = 46$. $\overline{u_1^2}(0) \simeq \overline{u_2^2}(0) \simeq \overline{u_3^2}(0) \simeq \frac{2}{3}u'^2$, the slight difference between $\overline{u_1^2}(0)$, $\overline{u_2^2}(0)$ and $\overline{u_3^2}(0)$ is due to the difficulty of generating an initial field that is exactly isotropic with a restricted number of discrete Fourier modes; note that for the same reason $\overline{u_1^2}(t)$ and $\overline{u_2^2}(t)$ are not exactly the same either, in fact their difference remains of the same order as that between $\overline{u_1^2}(0)$ and $\overline{u_2^2}(0)$.

We find, as expected, that $\overline{u_1^2} \simeq \overline{u_2^2} \simeq \overline{u_3^2} \simeq \frac{2}{3}u'^2$ at time $t = 0$, and that $\overline{u_1^2}$, $\overline{u_2^2}$ decrease towards a constant and $\overline{u_3^2}$ decreases and oscillates around a lower constant within one characteristic buoyancy time $2\pi/N$. This decrease in kinetic energy corresponds to an increase in potential energy, and these constants are in satisfactory agreement with the predictions of Hanazaki & Hunt (1996), namely that

$$\lim_{t\to\infty} \frac{\overline{u_1^2}(t)}{\overline{u_1^2}(0)} = \frac{\overline{u_2^2}(t)}{\overline{u_2^2}(0)} = \frac{7}{8}$$

and

$$\lim_{t\to\infty} \frac{\overline{u_3^2}(t)}{\overline{u_3^2}(0)} = \frac{1}{2}$$

when the initial potential energy is zero.

Hence, the Eulerian velocity field does indeed develop a well-defined anisotropy as a consequence of the stable stratification with a clear depletion of the turbulence in the vertical. Furthermore, once this depletion has set in, the flow is also effectively non-decaying. We release and track fluid elements to evaluate Lagrangian statistics after this depletion has set in.† Specifically we release the fluid elements in the stratified turbulence at times $t_0 = (10+\delta)2\pi/N$, where δ is a different random number between -1 and 1 for different trajectories in order to avoid an initial in-phase oscillation of all particles together and allow what may be a more realistic particle release.

To demonstrate that the Lagrangian turbulence is non-decaying and non-isotropic we have calculated the Lagrangian mean-square velocities as functions of time for a variety of Froude numbers all smaller than 1 since our model is not expected to be valid for Fr larger than 1. We use the notation $\boldsymbol{u}_L(t) = \boldsymbol{u}(\boldsymbol{x}(t), t)$ for Lagrangian velocities, and the Lagrangian mean-square velocity components that we have calcu-

† Godeferd *et al.* (1997) attempted a KS model of turbulent diffusion based on a EDQNM2 energy spectrum in order to introduce the anisotropy from the onset and not purely via the action of linear Boussinesq distortion. It is hard to comment on this paper however because it contains only one result obtained with KS without discussion of the limit of validity of Lagrangian calculations (Froude numbers, time ranges, etc).
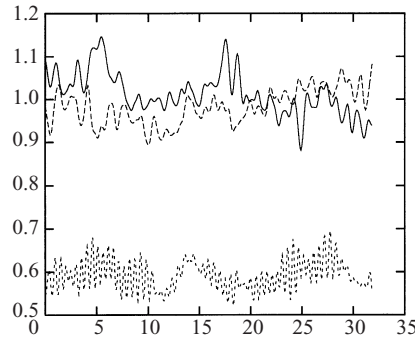
FIGURE 3. Non-dimensionalized KS Lagrangian mean-square velocities plotted against non-dimensionalized time $(t-t_0)N/2\pi$, $Fr = 0.0085$, $Lk_{max} = 46$ and the KS uses 20 000 modes. The ensemble average $\langle\cdots\rangle$ is taken over 20 trajectories from 40 different realizations. The convention is as follows: continuous line $\langle u_{L1}^2\rangle / \overline{u_1^2}(\infty)$, dash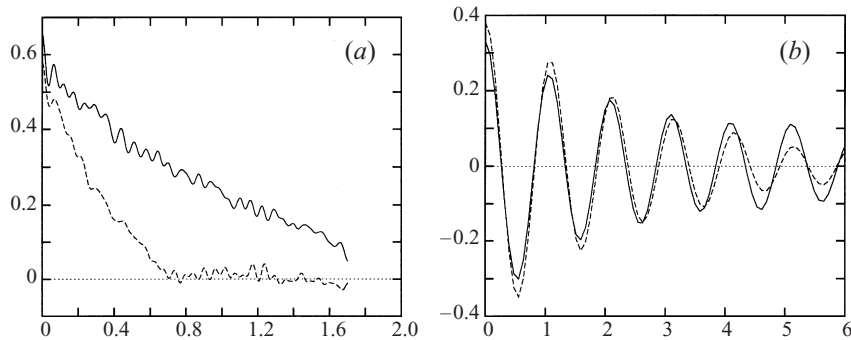ed line $\langle u_{L2}^2\rangle / \overline{u_1^2}(\infty)$, and dotted line $\langle u_{L3}^2\rangle / \overline{u_1^2}(\infty)$.

FIGURE 4. Non-dimensionalized KS Lagrangian velocity correlations for the same case as in figure 3. (a) Horizontal velocity correlation $\langle u_{L1}(t_0)u_{L1}(t_0 + t)/u'^2\rangle$ as a function of non-dimensionalized time $(t-t_0)u'/L$. (b) Vertical velocity correlation $\langle u_{L3}(t_0)u_{L3}(t_0 + t)\rangle/u'^2$ as a function of non-dimensionalized time $(t-t_0)N/2\pi$. Continuous line: $\lambda = 0$, dashed line: $\lambda = 1$.

lated are $\langle u_{L1}^2(t)\rangle$, $\langle u_{L2}^2(t)\rangle$, $\langle u_{L3}^2(t)\rangle$ where the brackets $\langle\cdots\rangle$ signify an average taken over twenty Lagrangian trajectories in forty different realizations of the turbulent-like velocity field. A representative example of our results is given in figure 3 where the time-axis is non-dimensionalized with $2\pi/N$. We find that all three mean-square velocity components fluctuate around a constant value which is almost the same for $\langle u_{L1}^2(t)\rangle$ and $\langle u_{L2}^2(t)\rangle$ but is clearly smaller for $\langle u_{L3}^2(t)\rangle$. This is a demonstration that the Lagrangian turbulence is non-decaying and that it is also non-isotropic in the sense that the Lagrangian kinetic energy is depleted in the direction of stratification.

We have also calculated the Lagrangian correlations $\langle u_{L1}(t_0)u_{L1}(t)\rangle$, $\langle u_{L2}(t_0)u_{L2}(t)\rangle$ and $\langle u_{L3}(t_0)u_{L3}(t)\rangle$ as functions of time and find that whereas $\langle u_{L1}(t_0)u_{L1}(t)\rangle$ and $\langle u_{L2}(t_0)u_{L2}(t)\rangle$ are the same within statistical errors, $\langle u_{L3}(t_0)u_{L3}(t)\rangle$ displays a very different behaviour characterized by well-defined regular oscillations of frequency N (see figure 4a, b). However, in the horizontal plane normal to the direction of stratification the Lagrangian integral time scale is significantly larger than L/u'. As can be seen in figure 4(a), the Lagrangian decorrelation in the horizontal plane is rather slow. Following Fung & Vassilicos (1998) and Malik & Vassilicos (1999) it is possible to increase this degree of decorrelation in the model and we introduce in every mode of the velocity field the option of an extra time oscillation of frequency

proportional to the eddy turnover frequency $\sqrt{k_n^3 E(k_n)}$ of the mode. Specifically, we replace (5.2) with

$$\boldsymbol{u}(\boldsymbol{x},t) = 2\pi \operatorname{Re}\left\{ \sum_{n=1}^{N_k} \sum_{m=1}^{M_\theta} k_n^2 \sin\theta_m \Delta k_n \Delta\theta_m \mathrm{e}^{\mathrm{i}(\boldsymbol{k}_{\mathrm{mn}}\cdot\boldsymbol{x}+\omega_{mn}t)} \right.$$
$$\left. \times [\tilde{v}_1(\boldsymbol{k}_{mn},t)\boldsymbol{c}_1(\boldsymbol{k}_{mn}) + \tilde{v}_2(\boldsymbol{k}_{mn},t)\boldsymbol{c}_2(\boldsymbol{k}_{mn})] \right\} \quad (5.5)$$

where $\omega_{mn} = \lambda\sqrt{k_n^3 E(k_n)}$ and in this paper we investigate both options, $\lambda = 1$ and $\lambda = 0$.

Some discussion is in order at this stage. The oscillations of frequency $\omega_{mn} = \sqrt{k_n^3 E(k_n)}$ may be interpreted as modelling the Lagrangian decorrelating effect of the nonlinear advection which we have neglected in our treatment of the Boussinesq equations. Indeed this linear approximation is satisfactory in the limit $Fr_\eta \ll 1$; however in the same limit, the eddy turnover frequencies $\sqrt{k_n^3 E(k_n)} \ll N$ so that the replacement of (5.2) by (5.5) may be expected to introduce the desired Lagrangian decorrelation in the horizontal plane without destroying the well-defined regular vertical Lagrangian oscillation of frequency N. Our results, examples of which are plotted in figure 4, justify this expectation. Note in particular that with the introduction of the frequencies ω_{mn} in $\boldsymbol{u}(\boldsymbol{x},t)$, $\langle u_{L1}(t_0)u_{L1}(t)\rangle$ drops down to 0 at about $t - t_0 \simeq L/u'$ (see figure 4a and the same holds for $\langle u_{L2}(t_0)u_{L2}(t)\rangle$), whilst the frequency N oscillations in $\langle u_{L3}(t_0)u_{L3}(t)\rangle$ remain largely unaffected even though some extra decorrelation has also been introduced in the direction of stratification (see figure 4b).

In the two sections that follow we report the results concerning one- and two-particle statistics obtained with our KS model of turbulent diffusion for high Reynolds number and low Froude number non-decaying turbulence.

6. One-particle turbulent diffusion

The KS model of turbulent diffusion in stably stratified non-decaying turbulence can be used to calculate diffusion in both horizontal and vertical directions concurrently and in agreement with incompressibility trajectory by trajectory. We have seen in §5 that for $t > t_0$ horizontal Lagrangian velocities are statistically stationary in the sense that $\langle u_{L1}^2(t)\rangle$ and $\langle u_{L2}^2(t)\rangle$ remain constant in time, and from now on we use the notation $\tau = t - t_0$. As shown by Taylor (1921), stationarity of Lagrangian statistics and a finite integral time scale T_L imply

$$\langle (x_i(\tau) - x_i(0))^2 \rangle \simeq \langle u_{Li}^2 \rangle \tau^2 \quad \text{for} \quad \tau \ll T_L, \quad (6.1)$$

and

$$\langle (x_i(\tau) - x_i(0))^2 \rangle \simeq 2\langle u_{Li}^2 \rangle T_L \tau \quad \text{for} \quad \tau \gg T_L, \quad (6.2)$$

where $i = 1, 2$.

The laws (6.1) and (6.2) are indeed observed in our KS (see figures 5a and 6a), both when $\lambda = 0$ and $\lambda = 1$. When $\lambda = 0$ T_L is significantly larger than L/u', but when $\lambda = 1$ T_L is about equal to L/u'. We have verified that T_L scales with L/u' both for $\lambda = 0$ and $\lambda = 1$ and that the KS model yields (see figures 5a and 6a)

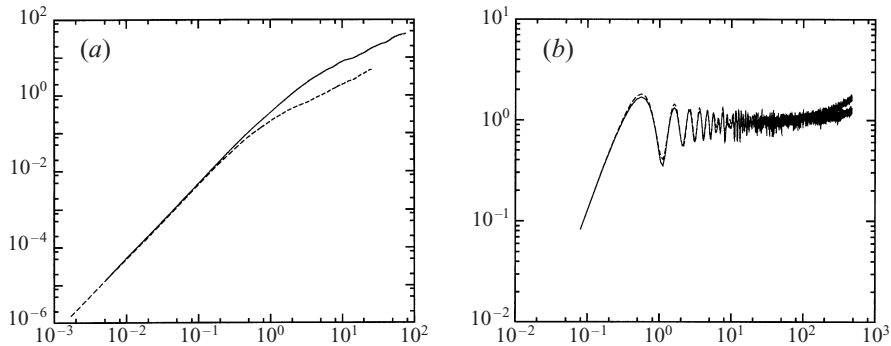$$\langle (x_i(\tau) - x_i(0))^2 \rangle \sim u'^2 \tau^2 \quad \text{for} \quad \tau \ll \frac{L}{u'} \quad (6.3)$$

FIGURE 5. One-particle turbulent diffusion obtained for $Fr = 0.0034$ and $Lk_{max} = 47$, for steady case $\lambda = 0$ (continuous line) and unsteady case $\lambda = 1$ (dashed line). (a) $(1/L^2)\langle(x_1(\tau) - x_1(0))^2\rangle$ as a function of $\tau u'/L$, (b) $\langle(x_3(\tau) - x_3(0))^2\rangle N^2/u'^2$ as a function of $\tau N/2\pi$. Notice that our simulations lose their accuracy after a few hundred buoyancy cycles, i.e. after a time between $100(2\pi/N)$ and $500(2\pi/N)$ according to the Froude number considered in this study. In this figure it is about $200(2\pi/N)$.
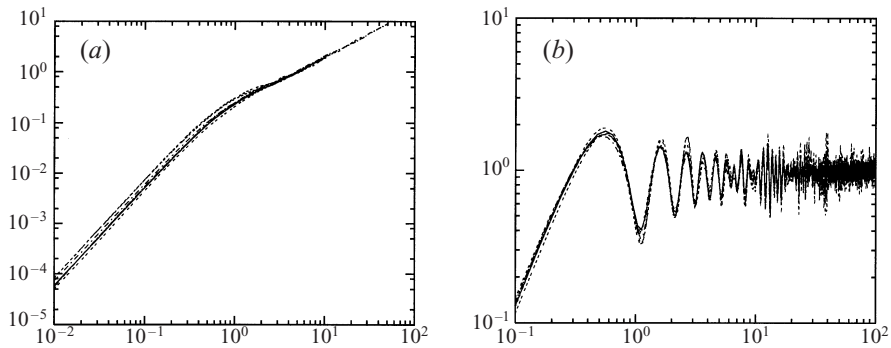
FIGURE 6. One-particle turbulent diffusion obtained from KS with $\lambda = 1$ for different values of Froude and Reynolds numbers (either changing N or u'/L or both): $Fr = 0.0034$, $Lk_{max} = 47$ and $\Delta_0 k_{max} = 0.1$; $Fr = 0.0034$, $Lk_{max} = 47$ and $\Delta_0 k_{max} = 0.2$; $Fr = 0.0034$, $Lk_{max} = 47$ and $\Delta_0 k_{max} = 0.4$; $Fr = 0.0017$, $Lk_{max} = 47$ and $\Delta_0 k_{max} = 0.2$; $Fr = 0.0011$, $Lk_{max} = 47$ and $\Delta_0 k_{max} = 0.2$; $Fr = 0.0034$, $Lk_{max} = 78$ and $\Delta_0 k_{max} = 0.2$; $Fr = 0.0028$, $Lk_{max} = 22$ and $\Delta_0 k_{max} = 0.2$; $Fr = 0.00064$, $Lk_{max} = 146$ and $\Delta_0 k_{max} = 0.2$; $Fr = 0.0017$, $Lk_{max} = 77$ and $\Delta_0 k_{max} = 0.1$. (a) $(1/L^2)\langle(x_1(\tau) - x_1(0))^2\rangle$ as a function of $\tau u'/L$, (b) $\langle(x_3(\tau) - x_3(0))^2\rangle N^2/u'^2$ as a function of $\tau N/2\pi$.

and

$$\langle(x_i(\tau) - x_i(0))^2\rangle \sim u'L\tau \quad \text{for} \quad \tau > \frac{L}{u'}. \tag{6.4}$$

Hence, horizontal one-particle diffusion is found to have no dependence on N for both $\lambda = 0$ and $\lambda = 1$.

In the vertical direction we retrieve the law (6.3) but for $\tau \ll 2\pi/N$ (and $i = 3$). However, for larger times our results reveal a strong depletion in vertical diffusion which is about the same for $\lambda = 0$ and $\lambda = 1$ (figure 5b). Having run this KS model for many different cases (different Froude and Reynolds numbers), all such that $Fr < 1$, we find that $\langle(x_3(\tau) - x_3(0))^2\rangle$ oscillates around the constant value

$$\langle(x_3(\tau) - x_3(0))^2\rangle \simeq \frac{u'^2}{N^2} = L^2 Fr^2 \quad \text{for} \quad \frac{2\pi}{N} \ll \tau \tag{6.5}$$

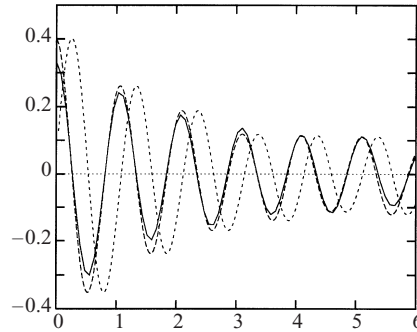for both $\lambda = 0$ and $\lambda = 1$ (see figures 5b and 6b).

FIGURE 7. $Fr = 0.0028$, $Lk_{max} = 22$, $\lambda = 1$. Continuous line: Lagrangian velocity correlation $\langle u_{L3}(t_0)u_{L3}(t_0+t)\rangle/u'^2$, dotted line: $\langle (a_3 - g\Theta_0)\dot{x}_3\rangle/Nu'^2$. Dashed line: $\langle (a_3 - g\Theta_0)\dot{x}_3\rangle/Nu'^2$ translated in time to collapse with $\langle u_{L3}(t_0)u_{L3}(t_0 + t)\rangle/u'^2$. The abscissa is non-dimensional time $N\tau/2\pi$.

A number of attempts to explain this capping of vertical one-particle-diffusion and to predict the scaling (6.5) can be found in the literature. Most recently, Kaneda & Ishida (2000) have obtained (6.5) by using the linearised Boussinesq equations and Corrsin's approximation. A very physical attempt is the one by Pearson *et al.* (1983) who invoked equipartition between average kinetic and potential vertical energies. A related approach may be based on the conservation of energy, and we discuss this approach first before addressing vertical equipartition (see also van Haren 1993 for a different concept of equipartition).

Multiplying (2.8) by $\dot{z}$ (from now on we use the notation $z = x_3(\tau) - x_3(0)$ and $\Theta_0 = \Theta(t_0)$) and integrating once gives the one-dimensional energy conservation along the vertical

$$\tfrac{1}{2}\dot{z}^2 + \tfrac{1}{2}N^2z^2 = \int_{\tau=0}^{\tau} (a_3 - g\Theta_0)\dot{z}\,\mathrm{d}t' + \tfrac{1}{2}\dot{z}(0)^2. \qquad (6.6)$$

Then, averaging and making use of $\langle \dot{z}^2(\tau)\rangle = \langle \dot{z}(0)^2\rangle$ for $\tau > 0$ yields

$$N^2\langle z(\tau)^2\rangle = 2\int_{\tau=0}^{\tau} \langle (a_3 - g\Theta_0)\dot{z}\rangle\,\mathrm{d}t'. \qquad (6.7)$$

The capping of one-particle vertical diffusion is therefore related to the Lagrangian correlation between the pressure acceleration $a_3 - g\Theta_0$ and the vertical velocity. We find that $\langle (a_3 - g\Theta_0)\dot{z}\rangle$ can be made to collapse with $N\langle u_{L3}(0)u_{L3}(\tau)\rangle$ in our KS by a simple translation in time (see figure 7). A time integration of results such as that of figure 4(b) leads to

$$\int_{\tau=0}^{\tau} \langle u_{L3}(0)u_{L3}(\tau)\rangle\,\mathrm{d}\tau = 0 \qquad (6.8)$$

for $\tau N \gg 2\pi$ but because of the time shift that distinguishes between $\langle (a_3 - g\Theta_0)\dot{z}\rangle$ and $N\langle u_{L3}(0)u_{L3}(\tau)\rangle$, it turns out that

$$\int_{\tau=0}^{\tau} \mathrm{d}t' \langle (a_3 - g\Theta_0)\dot{z}\rangle \simeq \tfrac{1}{2}u'^2 \qquad (6.9)$$

for $\tau \gg 2\pi/N$. The capping of vertical diffusion with the right scaling (6.5) follows from (6.7) and (6.9).

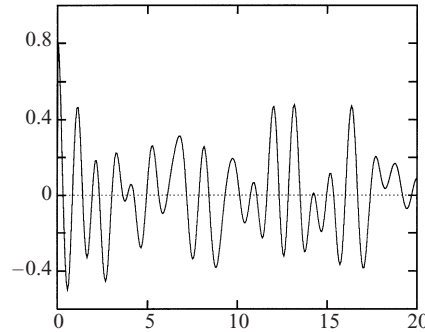David Thomson (April 1999, private communication) derives the capping of one-

FIGURE 8. $(g^2/N^2)\langle\Theta_0\Theta(t)\rangle/u'^2$ as a function of the non-dimensional time $\tau N/2\pi$. These oscillations around 0 are observed for the entire duration even of our longest simulations in time. $Fr = 0.00064$, $Lk_{max} = 146$, $\lambda = 1$.

particle diffusion and (6.5) from the conservation of energy, but in three dimensions rather than along the vertical direction only. From (2.4), (2.5) and (2.8) he gets

$$\frac{d}{dt}\left(\langle\tfrac{1}{2}|\boldsymbol{u}_L|^2\rangle + \frac{N^2}{2}\langle z^2\rangle\right) = \langle\boldsymbol{a}\cdot\boldsymbol{u}_L\rangle - g\langle\Theta_0\dot{z}\rangle \qquad (6.10)$$

and he then argues on the basis of statistical homogeneity that the Lagrangian average $\langle\boldsymbol{a}\cdot\boldsymbol{u}_L\rangle$ is equal to the Eulerian average of $(1/\rho)\boldsymbol{u}\cdot\nabla p'$ which vanishes by incompressibility and homogeneity. As stated in §5 and shown in figure 3, $(d/dt)\langle\tfrac{1}{2}|\boldsymbol{u}_L|^2\rangle$ also vanishes for $t > t_0$, so that one is left with

$$\frac{d}{dt}\frac{N^2}{2}\langle z^2\rangle = -g\langle\Theta_0\dot{z}\rangle. \qquad (6.11)$$

(See also Pearson 1980 for a three-dimensional argument and explanation of the capping of vertical one-particle diffusion based on (6.11).) Because $\langle\Theta_0\dot{z}\rangle = (d/dt)\langle\Theta_0 z\rangle$ and $z(\tau = 0) = 0$, integration of (6.11) from 0 to τ leads to

$$\frac{N^2}{2}\langle z^2\rangle = -g\langle\Theta_0 z\rangle. \qquad (6.12)$$

Finally the Schwartz inequality $\langle\Theta_0 z\rangle^2 \leqslant \langle\Theta_0^2\rangle\langle z^2\rangle$ implies that

$$\langle z^2\rangle \leqslant 4g^2\frac{\langle\Theta_0^2\rangle}{N^4}. \qquad (6.13)$$

In the present KS model's linear Boussinesq approximation where $\langle\Theta_0^2\rangle = \tfrac{1}{2}u'^2 N^2/g^2$ (a special case of equation (3.24d) in Hanazaki & Hunt 1996), (6.12) leads to (6.5) by using $\Theta(t) - \Theta_0 = (N^2/g)z(t)$ (which follows from (2.7)), if and only if the assumption is made that $\langle\Theta(t)\Theta_0\rangle \simeq 0$ or at least oscillates around 0 for $\tau \gg 2\pi/N$. We have been able to confirm the validity of this assumption in our KS to the extent that $\langle\Theta(t)\Theta_0\rangle$ is indeed found to oscillate around 0 (see figure 8).

To summarize, formula (6.5) for the capping of vertical one-particle diffusion can be obtained from one-dimensional energy conservation along the vertical if use is made of $\int_0^\tau\langle(a_3 - g\Theta_0)\dot{z}\rangle\,dt' = \tfrac{1}{2}u'^2$ which we have observed to hold in our KS model. However (6.5) can also be obtained from three-dimensional energy conservation without such detailed input concerning the correlation between vertical Lagrangian pressure acceleration and vertical Lagrangian velocity, but by recourse to the relation $\langle\Theta(t)\Theta_0\rangle \simeq 0$ for large τ. We now show that (6.5) is not a consequence of vertical
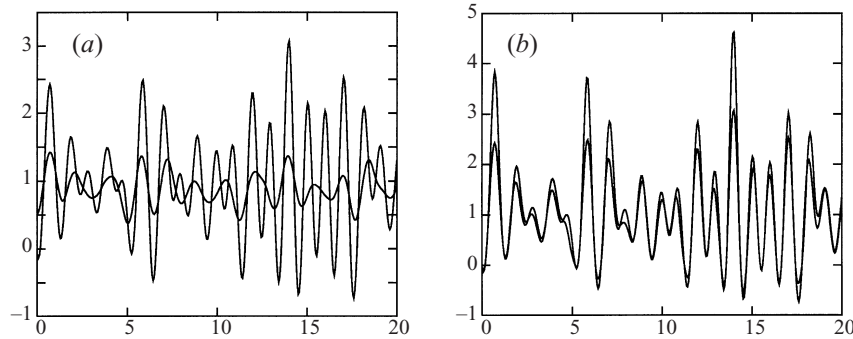
FIGURE 9. An arbitrary trajectory from an arbitrary realization, $Fr = 0.0028$, $Lk_{max} = 22$, $\lambda = 0$ but effectively the same results are obtained with $\lambda = 1$. (a) Thicker line: $(x_3(\tau) - x_3(0))N/u'$, thinner line: $(a_3 - g\Theta_0)u'/N$. (b) Thicker line: $(x_3(\tau) - x_3(0))N/u'$, thinner line: $(a_3 - g\Theta_0)(x_3(\tau) - x_3(0))1/u'^2$. The abscissa is non-dimensional time $\tau N/2\pi$ in both plots.

equipartition between average kinetic and potential energies, simply because such equipartition does not hold.

To derive such equipartition from first principles, one multiplies (2.8) by z leading to

$$\tfrac{1}{2}\dot{z}^2 - \frac{N^2}{2}z^2 = \frac{1}{2}\frac{\mathrm{d}^2}{\mathrm{d}\tau^2}\left(\frac{z^2}{2}\right) - \tfrac{1}{2}(a_3 - g\Theta_0)z. \tag{6.14}$$

Vertical equipartition is the property that

$$\tfrac{1}{2}\langle\dot{z}^2\rangle = \frac{N^2}{2}\left\langle\left(z + g\frac{\Theta_0}{N^2}\right)^2\right\rangle$$

(the potential energy is defined in terms of the departure from the equilibrium height where $\Theta = 0$), and a necessary and sufficient condition for it to hold is

$$\left\langle\frac{\mathrm{d}^2}{\mathrm{d}\tau^2}\frac{z^2}{2}\right\rangle = \langle(a_3 - g\Theta_0)z\rangle + 2g\langle z\Theta_0\rangle + \frac{g^2}{N^2}\langle\Theta_0^2\rangle.$$

Hence if vertical equipartition between average kinetic and potential energies is to coexist with the capping of vertical diffusion we should expect

$$\langle(a_3 - g\Theta_0)z\rangle + 2g\langle z\Theta_0\rangle + \frac{g^2}{N^2}\langle\Theta_0^2\rangle$$

to vanish (or more precisely to oscillate around 0). As illustrated in figure 9, $(a_3 - g\Theta_0)$ and z turn out to be strongly correlated and $(a_3 - g\Theta_0)z/u'^2$ oscillates in time in a way very close to zN/u' for every trajectory, albeit with more amplification. In figure 10 we plot Lagrangian averages of $a_3 - g\Theta_0$, z, z^2 and $(a_3 - g\Theta_0)z$ and we find, in particular, that

$$\langle(a_3 - g\Theta_0)z\rangle = \frac{2N^2}{3}\langle z^2\rangle$$

for $\tau > 0$. Hence, vertical equipartition becomes equivalent to the requirement that

$$\frac{2N^2}{3}\langle z^2\rangle + 2g\langle z\Theta_0\rangle + \frac{g^2}{N^2}\langle\Theta_0^2\rangle = 0$$
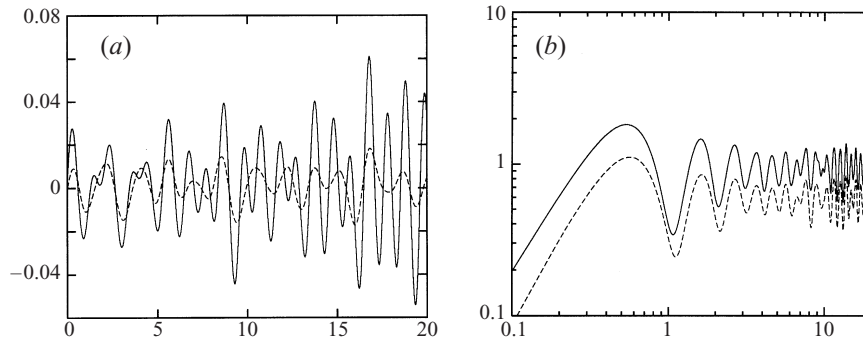
FIGURE 10. $Fr = 0.0028$, $Lk_{max} = 22$, $\lambda = 0$ but effectively the same results are obtained with $\lambda = 1$. (a) Continuous line: $\langle x_3(\tau) - x_3(0) \rangle N/u'$, dashed line: $\langle a_3(\tau) - g\Theta_0 \rangle u'/N$. (b) Logarithmic plot, continuous line: $\langle (x_3(\tau) - x_3(0))^2 \rangle N^2/u'^2$, dashed line: $\langle (a_3 - g\Theta_0)(x_3 - x_3(0)) \rangle 1/u'^2$. The abscissa is non-dimensional time $\tau N/2\pi$ in both plots.

which is in turn equivalent to

$$\langle z^2 \rangle = \frac{3}{2} \frac{u'^2}{N^2}$$

(not (6.5)!) on account of (6.12) and $\langle \Theta_0^2 \rangle = \frac{1}{2} u'^2 N^2/g^2$ (Hanazaki & Hunt 1996). Our numerical observations $\langle (a_3 - g\Theta_0)z \rangle = \frac{2}{3} N^2 \langle z^2 \rangle$ and $\langle z^2 \rangle = u'^2/N^2$ combined are therefore evidence that there is no vertical equipartition between kinetic and potential energies. In fact, as we show in the next paragraph, $\langle (a_3 - g\Theta_0)z \rangle = \frac{2}{3} N^2 \langle z^2(t) \rangle$ implies $\langle z^2(t) \rangle = \frac{1}{2} u'^2$.

Taking a Lagrangian average of (6.14), using $\langle (a_3 - g\Theta_0)z \rangle = \frac{2}{3} N^2 \langle z^2 \rangle$ and the result of Hanazaki & Hunt (1996) which we have confirmed in figure 2, namely that $\langle \dot{z}(\tau)^2 \rangle = \frac{1}{3} u'^2$ $(= \frac{1}{2} \overline{u_1^2}(t = 0))$ for $\tau \gg 2\pi/N$, we obtain a linear second-order differential equation for $\langle z^2 \rangle$ that is valid for $\tau \gg 2\pi/N$:

$$\frac{3}{2} \frac{\mathrm{d}^2}{\mathrm{d}\tau^2} \langle z^2 \rangle + N^2 \langle z^2 \rangle = u'^2. \tag{6.15}$$

The solution of this equation is $\langle z^2 \rangle = (u'^2/N^2) +$ an oscillation of frequency proportional to N, in agreement with our finding (6.5). We can say that it is because $\langle (a_3 - g\Theta_0)z \rangle = \frac{2}{3} N^2 \langle z^2 \rangle$ that we have a well-defined capping of the vertical diffusion without vertical equipartition.

The second category of attempts to explain and predict the scaling of $\langle z^2 \rangle$ is based on assumptions concerning the statistics of a_3 and special values for Θ_0. In these attempts (Csanady 1964; Pearson *et al.* 1983; Kimura & Herring 1996) Θ_0 is taken equal to 0 for all the trajectories and a_3 is modelled in terms of a white noise, either by specifying a delta-correlation in time or by improving a flat power spectrum. Hence, it is invariably effectively assumed that $a_3 - g\Theta_0$ is statistically uncorrelated with both $z(\tau)$ and $\dot{z}(\tau)$. In this KS model, and presumably also in reality, the Lagrangian acceleration $a_3 - g\Theta_0$ is very significantly correlated with the vertical displacement and the Lagrangian velocity, and such assumptions are therefore inappropriate.

It may be of some interest to draw this discussion of the capping of vertical diffusion to a close with the following remark. By virtue of incompressibility the pressure acceleration is given by (3.7) and is therefore modulated by the buoyancy

force. Incompressibility is incorporated in our KS model trajectory by trajectory and so is therefore the coupling between a_3 and the buoyancy force. From the quantitative expression of this coupling, (3.7), it follows that

$$|a_3(\tau)| \leqslant N \int d\boldsymbol{k} \frac{k_3^2}{k^2} |\tilde{v}_2(\boldsymbol{k}, t_0)| \tag{6.16}$$

implying that $|a_3(\tau)|$ is bounded at all times by a constant independent of time in our KS model. The existence of an upper bound for $|a_3(\tau)|$ implies an upper bound on $|z(\tau)|$ for *every single trajectory*. The proof of this statement proceeds from (2.8) which we can square to write

$$|\ddot{z}|^2 + N^4|z|^2 + 2\ddot{z}N^2z = |a_3 - g\Theta_0|^2. \tag{6.17}$$

If $|a_3(\tau)|$, and therefore $|a_3 - g\Theta_0|^2$, are bounded from above, then, because $|\ddot{z}|^2$ is positive, $|z|^2$ cannot grow to $+\infty$ without $2\ddot{z}N^2z$ tending to $-\infty$. This means that if $z \to +\infty$, $\ddot{z}$ should tend to $-\infty$ which is impossible and if $z \to -\infty$, $\ddot{z}$ should tend to $+\infty$ which is also impossible. Hence an upper bound for $|a_3(\tau)|$ implies an upper bound for $|z|$ for every trajectory.

However, it must be pointed out that (2.8), and therefore also (6.17), are not rigourously accurate representations of particle motion generated by the velocity field (3.3) (3.4) (3.5) which has been obtained by solving the *linear* Boussinesq equations. The Lagrangian equation (2.8) is rigorously compatible only with the *nonlinear* Boussinesq equations. Nevertheless for small Froude numbers and for times τ smaller than about L/u' we can expect (2.8) to be valid in the context of our KS model. This is indeed the case: it is on the basis of (2.8) that we have shown (6.5) and (6.9) to be equivalent, and they are both obtained in our simulations; it is also because of (2.8) and the linear approximation results $\langle \Theta_0^2 \rangle = \frac{1}{2}u'^2N^2/g^2$ that $\langle \Theta(t)\Theta_0 \rangle$ oscillates around 0 if and only if $\langle z^2 \rangle$ oscillates around u'^2/N^2, and again both these oscillatory behaviours are quite faithfully observed in our simulations; and it is because of (2.8) and $\langle \dot{z}^2(0) \rangle = \frac{1}{3}u'^2$ that (2.8) is equivalent to $\langle (a_3 - g\Theta_0)z \rangle = \frac{2}{3}N^2\langle z^2 \rangle$ which is once again clearly observed in our KS.

All the laws just mentioned are however observed up to times τ of about one or a few L/u', and our evidence indicates that they may break down in our simulations for times larger than this, as can be seen for example at the right-hand side of figure 5(*b*) (particularly, as may be expected, for $\lambda = 1$). The capping of vertical diffusion which is well represented by linear mechanisms up to a time $O(L/u')$, may (or may not) require nonlinear mechanisms to be sustained beyond times $O(L/u')$. This is a question we cannot answer in this paper. That the capping of vertical diffusion must hold for all times follows from David Thomson's inequality (6.13).

In the linear approximation of the Boussinesq equations we can show that $|a_3|$ is bounded for all times, but (6.17) is not guaranteed to be valid for very long times. However, we can safely state that for the full nonlinear Boussinesq equations we have shown that if $|a_3|$ is bounded, so is $|z|$ for every Lagrangian particle trajectory.

7. Two-particle turbulent diffusion

We integrated twenty pairs of particle trajectories $\boldsymbol{x}^{(1)}(t)$ and $\boldsymbol{x}^{(2)}(t)$ in forty realizations of the KS non-decaying stratified turbulence detailed in §5. The particle pairs were initially all either in a horizontal plane or along the same vertical straight line with the same initial separation $\Delta_0 = |\boldsymbol{x}^{(1)}(t_0) - \boldsymbol{x}^{(2)}(t_0)|$. Both configurations give the same results and for economy of space we only present the results corresponding to
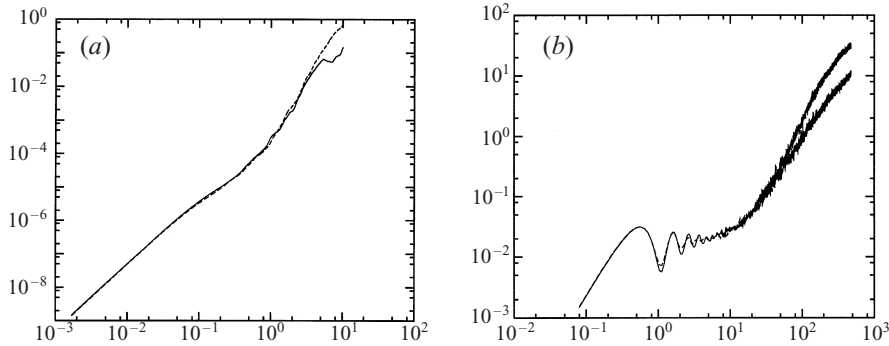
FIGURE 11. Two-particle turbulent diffusion obtained for $Fr = 0.0034$ and $Lk_{max} = 47$, for steady case $\lambda = 0$ (continuous line) and unsteady case $\lambda = 1$ (dashed line). (a) $\langle \Delta x_1^2 \rangle / L^2$ as a function of $\tau u'/L$, (b) $\langle \Delta x_3^2 \rangle N^2/(u' \Delta_0^2)$ as a function of $\tau N/2\pi$.

particle pairs initially in a horizontal plane. We have also compared results for $\lambda = 0$ and $\lambda = 1$; figure 11 is evidence that two-particle diffusion in the horizontal plane (figure 11a) and along the vertical direction (figure 11b) is the same for both values of λ, and the different laws and régimes that we present in this section are effectively the same for both $\lambda = 0$ and $\lambda = 1$.

We have calculated the Lagrangian two-particle statistics $\langle \Delta x_1^2(t) \rangle$, $\langle \Delta x_2^2(t) \rangle$ and $\langle \Delta x_3^2(t) \rangle$ where $\Delta x(t) = (x^{(1)}(t) - x^{(1)}(t_0)) - (x^{(2)}(t) - x^{(2)}(t_0))$ and the averaging operation $\langle \cdots \rangle$ is the one defined in §5. Such runs were conducted for many different Froude and Reynolds numbers and different values of Δ_0 and our results are summarized in figures 12 and 13 for two-particle diffusion in the horizontal plane and figures 14, 15 and 16 for two-particle diffusion along the vertical axis x_3.

The results for $\langle \Delta x_1^2(t) \rangle$ and $\langle \Delta x_2^2(t) \rangle$ are about the same so we only plot those for $\langle \Delta x_1^2(t) \rangle$ (see figures 12 and 13). For small times τ (definitely much smaller than L/u', however possibly also much smaller than a length scale smaller than L/u', but we have not been able to determine this length scale, an issue which we leave open for future investigation) we find that

$$\langle \Delta x_1^2(\tau) \rangle \simeq \frac{\Delta_0^2}{L^2} \left(\frac{L}{\eta} \right)^{4/3} u'^2 \tau^2 \tag{7.1}$$

when $\Delta_0 < \eta$ (figures 12a) and

$$\langle \Delta x_1^2(\tau) \rangle \simeq u'^2 \left(\frac{\Delta_0}{L} \right)^{2/3} \tau^2 \tag{7.2}$$

when $\Delta_0 \geqslant \eta$ (figure 12b). One can expect from a straightforward Taylor expansion in the limit $\tau \ll L/u'$ that

$$\langle \Delta x_1^2(\tau) \rangle \simeq (\Delta V_0)^2 \tau^2 \tag{7.3}$$

where ΔV_0 is a characteristic velocity difference associated with the scale Δ_0. When $\Delta_0 < \eta$, ΔV_0 may be approximated by Δ_0 times a characteristic small-scale strain rate, and if we interpret this strain rate to scale as $(\epsilon/v)^{1/2}$ where ϵ is u'^3/L and v is related to η by $\eta \sim (v^3/\epsilon)^{3/4}$ then

$$\Delta V_0 \sim \frac{\Delta_0}{L} \left(\frac{L}{\eta} \right)^{2/3} u' \quad \text{for} \quad \Delta_0 < \eta \tag{7.4}$$
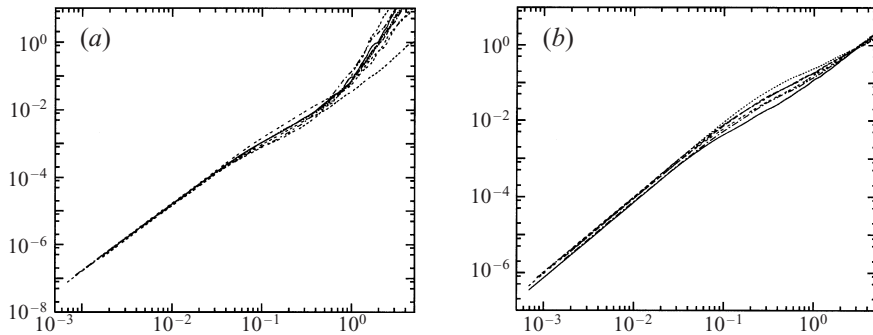
FIGURE 12. Small-time dependence of two-particle diffusion along horizontal direction x_1, pairs of particle are initially released in an horizontal plane. (a) $\Delta_0 < \eta$, $(\langle \Delta x_1^2 \rangle / \Delta_0^2)(Lk_{max})^{4/3}$ as function of $(u'/L)\tau$, and the different cases are: $Fr = 0.0034$, $Lk_{max} = 47$ and $\Delta_0 k_{max} = 0.1$; $Fr = 0.0034$, $Lk_{max} = 47$ and $\Delta_0 k_{max} = 0.2$; $Fr = 0.0034$, $Lk_{max} = 47$ and $\Delta_0 k_{max} = 0.4$; $Fr = 0.0017$, $Lk_{max} = 47$ and $\Delta_0 k_{max} = 0.2$; $Fr = 0.0011$, $Lk_{max} = 47$ and $\Delta_0 k_{max} = 0.2$; $Fr = 0.0034$, $Lk_{max} = 77$ and $\Delta_0 k_{max} = 0.2$; $Fr = 0.0028$, $Lk_{max} = 22$ and $\Delta_0 k_{max} = 0.2$; $Fr = 0.0017$, $Lk_{max} = 77$ and $\Delta_0 k_{max} = 0.1$; $Fr = 0.0034$, $Lk_{max} = 47$ and $\Delta_0 k_{max} = 0.2$. (b) $\langle \Delta x_1^2 \rangle (L/\Delta_0)^{2/3}$ as function of $(u'/L)\tau$ and the different cases are: $Fr = 0.0017$, $Lk_{max} = 77$ and $\Delta_0 k_{max} = 5$; $Fr = 0.0034$, $Lk_{max} = 47$ and $\Delta_0 k_{max} = 10$; $Fr = 0.0017$, $Lk_{max} = 47$ and $\Delta_0 k_{max} = 10$; $Fr = 0.0028$, $Lk_{max} = 22$ and $\Delta_0 k_{max} = 10$; $Fr = 0.0034$, $Lk_{max} = 47$ and $\Delta_0 k_{max} = 5$; $Fr = 0.0011$, $Lk_{max} = 47$ and $\Delta_0 k_{max} = 10$; $Fr = 0.0017$, $Lk_{max} = 77$ and $\Delta_0 k_{max} = 10$.
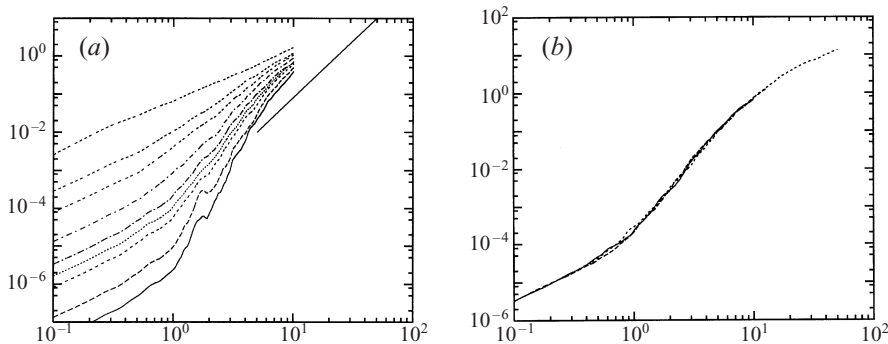

FIGURE 13. Two-particle turbulent diffusion along x_1 obtained from KS with $\lambda = 1$: $\langle \Delta x_1^2 \rangle / L^2$ as a function of $\tau u'/L$. (a) Results for fixed Froude and Reynolds numbers $Fr = 0.0034$ and $Lk_{max} = 47$ and different values of Δ_0, from top to bottom $\Delta_0 k_{max} = 10, 2, 1, 0.4, 0.2, 0.14, 0.1, 0.04, 0.02$. (b) Results for a given Δ_0 and Reynolds number, $\Delta_0 k_{max} = 0.2$ and $Lk_{max} = 47$ and different Froude numbers $Fr = 0.0037, 0.0017$ and 0.0011.

and the scaling (7.1) is recovered. When, however, $\Delta_0 > \eta$, a K41 type argument (see Frisch 1995, chap. 6) leads to

$$\Delta V_0 \sim u' \left(\frac{\Delta_0}{L} \right)^{1/3} \quad \text{for} \quad \Delta_0 > \eta \tag{7.5}$$

and the scaling (7.2) is recovered too.

It is also found (see figure 13b) that $\langle \Delta x_1^2(\tau) \rangle$ is independent of N for all times τ both smaller and larger than L/u'. For times $\tau > L/u'$ the two particles are statistically independent and we retrieve the large time relation

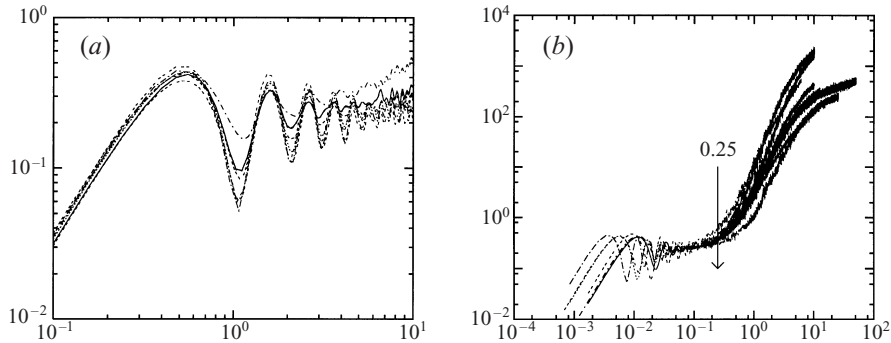$$\langle \Delta x_1^2(\tau) \rangle \simeq 2Lu'\tau. \tag{7.6}$$

FIGURE 14. Two-particle turbulent diffusion in the direction of stratification x_3 obtained from KS, $\lambda = 1$, for $\Delta_0 < \eta$ and the pairs of particles are released from an horizontal plane, different cases are those in figure 6: (a) $\langle \Delta x_3^2 \rangle / \Delta_0^2 Fr^2 (L/\eta)^{4/3}$ against $\tau N/2\pi$; (b) Same cases but with a different normalization $\langle \Delta x_3^2 \rangle / \Delta_0^2 Fr^2 (L/\eta)^{4/3}$ as a function of $\tau u'/L$. The arrow points at $\tau u'/L = 0.25$.

It should be noted that we do not observe a τ^3 scaling (see figure 13a) as Elliott & Majda (1996), Fung & Vassilicos (1998) and Flohr & Vassilicos (2000) do for isotropic turbulent-like velocity fields with a $-\frac{5}{3}$ energy spectrum. However, $L/\eta < 24$ here, which is much smaller than the ratio L/η required by Elliott & Majda (1996), Fung & Vassilicos (1998) and Flohr & Vassilicos (2000) to observe Richardson's τ^3 law over at least one or two or indeed many more decades.

Concerning two-particle diffusion along the vertical we expect that $|\Delta x_3|$ is bounded for all times and for every pair of trajectories simply because $|z|$ is bounded for all times and for every trajectory as we have shown in the previous section. This is indeed what we observe, but we also observe three different régimes in the time evolution of $\langle \Delta x_3^2(\tau) \rangle$. The first régime corresponds to times $\tau \ll 2\pi/N$ and in this range of small times

$$\langle \Delta x_3^2(\tau) \rangle \simeq \frac{\Delta_0^2}{L^2} \left(\frac{L}{\eta} \right)^{4/3} u'^2 \tau^2 \tag{7.7}$$

when $\Delta_0 < \eta$ (figure 14a, b) but

$$\langle \Delta x_3^2(\tau) \rangle \simeq u'^2 \left(\frac{\Delta_0}{L} \right)^{2/3} \tau^2 \tag{7.8}$$

when $\Delta_0 \geqslant \eta$ (figure 15a, b). Once again, these scalings can be reduced to the leading order of a Taylor expansion

$$\langle \Delta x_3^2(\tau) \rangle \simeq (\Delta V_0)^2 \tau^2 \quad \text{for} \quad \tau \ll \frac{2\pi}{N}, \tag{7.9}$$

with ΔV_0 given by (7.4) and (7.5). Note that, in this régime, $\langle \Delta x_3^2(\tau) \rangle$ does not depend on the Froude number and obeys the same scaling as diffusion in the horizontal plane.

A second régime is observed for $2\pi/N \ll \tau$ and τ smaller than a time scale itself smaller than or equal to L/u'; in this régime the two-particle diffusion reaches a plateau which is given by

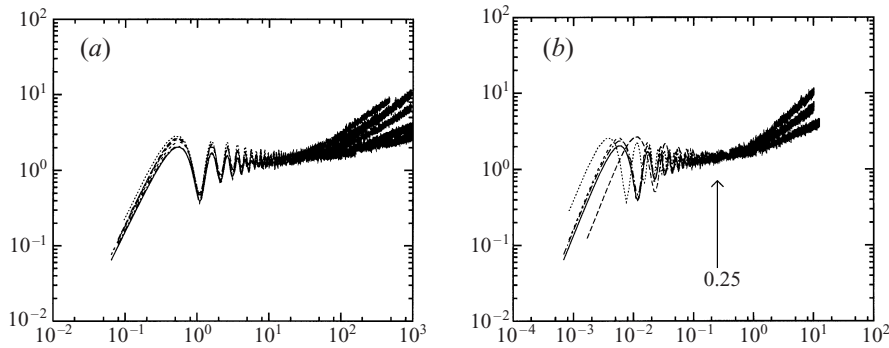$$\langle \Delta x_3^2(\tau) \rangle \simeq \Delta_0^2 Fr^2 \left(\frac{L}{\eta} \right)^{4/3} \tag{7.10}$$

FIGURE 15. Two-particle turbulent diffusion in the direction of stratification x_3 obtained from KS, $\lambda = 1$, for $\Delta_0 > \eta$ and the pairs of particles are released from an horizontal plane, different cases are: $Fr = 0.0017$, $Lk_{max} = 77$ and $\Delta_0 k_{max} = 5$, $Fr = 0.0034$, $Lk_{max} = 47$ and $\Delta_0 k_{max} = 10$, $Fr = 0.0017$, $Lk_{max} = 47$ and $\Delta_0 k_{max} = 10$, $Fr = 0.0030$, $Lk_{max} = 22$ and $\Delta_0 k_{max} = 10$, $Fr = 0.0034$, $Lk_{max} = 47$ and $\Delta_0 k_{max} = 5$, $Fr = 0.0011$, $Lk_{max} = 47$ and $\Delta_0 k_{max} = 10$, $Fr = 0.0017$, $Lk_{max} = 77$ and $\Delta_0 k_{max} = 10$. (a) $\langle \Delta x_3^2 \rangle (L/\Delta_0)^{2/3}(N/u')^2$ against $\tau N/2\pi$. (b) Same as (a) but with different normalizations: $\langle \Delta x_3^2 \rangle (L/\Delta_0)^{2/3}(N/u')^2$ against $\tau u'/L$. The arrow points at $\tau u'/L = 0.25$.

for $\Delta_0 < \eta$ (figure 14a, b) and

$$\langle \Delta x_3^2(\tau) \rangle \simeq \left(\frac{\Delta_0}{L} \right)^{2/3} L^2 Fr^2 \tag{7.11}$$

for $\Delta_0 \geqslant \eta$ (figure 15a, b). In terms of the characteristic velocity difference ΔV_0 given by (7.4) and (7.5), the two scalings (7.10) and (7.11) may be interpreted as deriving from the single scaling

$$\langle \Delta x_3^2(\tau) \rangle \simeq \frac{(\Delta V_0)^2}{N^2} \quad \text{when} \quad \frac{2\pi}{N} \ll t \ll \frac{L}{u'}. \tag{7.12}$$

Note that the scaling laws (7.10), (7.11) and (7.12) are valid modulo an oscillation around this average constant value $\Delta V_0^2/N^2$.

Finally, the third régime appears at large times $\tau \gg L/u'$, when the two particles become independent and we expect $\langle \Delta x_3^2(\tau) \rangle = 2\langle (x_3(\tau) - x_3(0))^2 \rangle$ $(= 2\langle z^2 \rangle)$. Assuming that (6.5) remains valid for times $\tau \gg L/u'$, it then follows from (6.5) that a second plateau is reached which is independent of Δ_0 and is given by

$$\langle \Delta x_3^2(\tau) \rangle \simeq 2L^2 Fr^2 \quad \text{when} \quad \frac{L}{u'} \ll \tau. \tag{7.13}$$

The beginning of this second plateau can be seen in figure 16 and more clearly in figure 17, but we were not able to carry out simulations with sufficient accuracy for times long enough to provide evidence for the coefficient 2 in (7.13). It can also be seen in figure 17 that the departure from the first two-particle diffusion plateau (7.12) to reach the second two-particle diffusion plateau (7.13) coincides with the time when the two particles start decorrelating in the horizontal plane, i.e. by the end of the two-particle τ^2 régime. A careful examination of figure 6 in Kimura & Herring (1996) and of a similar result by Heppe (1997) shows that the plateau in two-particle vertical diffusion observed by these authors is at a much smaller value than $2L^2 Fr^2 = 2u'^2/N^2$, in agreement with the first plateau observed in this paper. These authors did not take their simulations far enough in time to probe the existence of a second plateau.
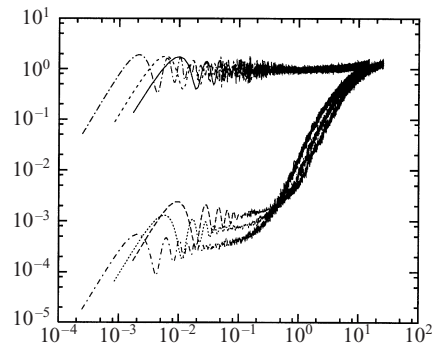
FIGURE 16. Comparison of one- and two-particle turbulent diffusions in the direction of stratification x_3 obtained from KS, $\lambda = 1$. Upper curves are $\langle(x_3(\tau) - x_3(0))^2\rangle N^2/u'^2$ against $\tau u'/L$, lower curves are $\langle\Delta x_3^2\rangle N^2/u'^2$ against $\tau u'/L$. The different cases are: $Fr = 0.0028$, $Lk_{max} = 22$ and $\Delta_0 k_{max} = 0.2$, $Fr = 0.0017$, $Lk_{max} = 47$ and $\Delta_0 k_{max} = 0.2$ and $Fr = 0.00064$, $Lk_{max} = 146$ and $\Delta_0 k_{max} = 0.2$.
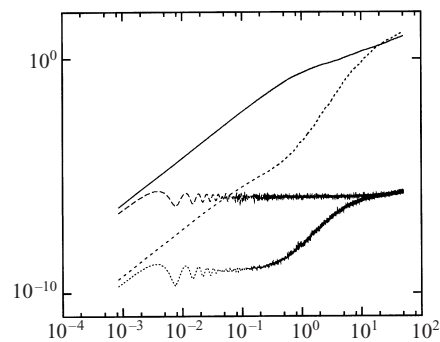

FIGURE 17. One- and two-particle diffusion, $Fr = 0.0011$ ($Fr_\eta = 0.02$), $Lk_{max} = 47$ and $\Delta_0 k_{max} = 0.2$. Solid line: $\langle x_1^2\rangle/L^2$, long dashed line: $\langle x_3^2\rangle/L^2$, short dashed line: $\langle\Delta x_1^2\rangle/L^2$, dotted line: $\langle\Delta x_3^2\rangle/L^2$; normalized time is $\tau u'/L$.

8. Conclusion

We have developed and used a KS Lagrangian model of turbulent diffusion in stably stratified non-decaying turbulence to predict one- and two-particle turbulent diffusion in both horizontal and vertical directions concurrently and in accordance with incompressibility trajectory by trajectory. Unlike Lagrangian stochastic models of turbulent diffusion in stably stratified turbulence, vertical and horizontal diffusion are not decoupled in this KS model. The present KS model has been developed for Reynolds numbers large enough to neglect the viscous terms in the Boussinesq equations, for times τ smaller than $O(L/u')$, for Froude numbers small enough to also neglect the nonlinear terms in the Boussinesq equations and for non-decaying stably stratified turbulence. The vanishing one- and two-particle vertical diffusivities (equations (6.5), (7.12) and (7.13)) are obtained for times $t - t_0 \gg 2\pi/N$ and in spite of the non-decaying mean-square vertical velocity. However this severe depletion of vertical diffusion is accompanied (but not explained!) by a reduced mean-square vertical velocity with respect to horizontal mean-square velocities (see also Vincent, Michaud & Meneguzzi 1996).

Our KS model's main results are illustrated in the summary figure 17. We have also shown that the capping of vertical diffusion is closely linked to the behaviour of the Lagrangian vertical pressure acceleration which is generated by the three-dimensional velocity field, and that this capping and its scalings are therefore accounted for by the full three-dimensional incompressible stratified flow. The Lagrangian vertical pressure acceleration is strongly correlated with the Lagrangian vertical position in such a way that $\langle z^2 \rangle = u'^2/N^2$ is accompanied by an absence of vertical equipartition between Lagrangian vertical potential and kinetic energies. In particular, in the context of the linear Boussinesq equations (which are used to develop the present KS model), the Lagrangian vertical pressure acceleration is bounded because the wavemodes of the horizontal and vertical velocity fields simply oscillate in time and are therefore bounded for all times. In the case of the nonlinear Boussinesq equations we have shown analytically that if the Lagrangian vertical acceleration a_3 is bounded for all times so is $z(t)$ for every trajectory. However, the proof that a_3 remains bounded in the nonlinear case is beyond the scope of the present paper.

Two-particle vertical diffusion displays two different plateaux, and the transition between the two plateaux corresponds to the time when particle pairs start moving apart in the horizontal, significantly enough for the τ^2 short-time laws (7.7) and (7.8) to break down. Furthermore, the scaling of the first two-particle vertical diffusion plateau depends on whether Δ_0 is larger or smaller than η. The second two-particle vertical diffusion plateau occurs much later in time when the two particles have become statistically uncorrelated, and is therefore independent of Δ_0 and η and equal to twice the one-particle vertical diffusion plateau, i.e. $2u'^2/N^2$.

David Thomson's inequality (6.13) shows that vertical diffusion must be capped for all times, at least when the effects of molecular diffusivity are neglected. Our KS model is based on the linear Boussinesq equations and can reproduce this capping of diffusion along with $\langle z^2 \rangle = u'^2/N^2$ up to a time of order L/u'. From times larger than $O(L/u')$, nonlinear effects may (or may not) become important, and the capping of vertical diffusion may require these nonlinear effects to persist. Hence, the full explanation of $\langle z^2 \rangle = u'^2/N^2$ for long times remains a challenge and this challenge must be addressed in a much broader context where both decaying and non-decaying stratified turbulence are considered, and where the effects of molecular diffusivity are incorporated too. To this challenge, this paper adds the task of explaining the two-plateaux structure of two-particle vertical diffusion.†

† We have obtained preliminary results which show that our conclusions concerning the existence of cappings for one- and two-particle diffusions, including the double-plateau structure of two-particle diffusion, are qualitatively unaffected by the precise form of the large-wavenumber energy spectrum.

REFERENCES

Britter, R. E., Hunt, J. C. R., Marsh, G. L. & Snyder, W. H. 1983 The effects of stable stratification on turbulent diffusion and the decay of grid turbulence. *J. Fluid Mech.* **127**, 27–44.

Csanady, G. T. 1964 Turbulent diffusion in a stratified fluid. *J. Atmos. Sci.* **21**, 439–447.

Dop, H. van, Nieuwstadt, F. T. M. & Hunt, J. C. R. 1985 Random-walk models for particle displacements in homogeneous unsteady turbulent flows. *Phys. Fluids* **28**, 1639–1653.

Elliott, F. W. & Majda, A. J. 1996 Pair dispersion over an intertial range spanning many decades. *Phys. Fluids* **8**, 1052–1060.

Flohr, P. & Vassilicos, J. C. 2000 Scalar subgrid model with flow structure for large-eddy simulations of scalar variances. *J. Fluid Mech.* **407**, 315–349.

Frisch, U. 1995 *Turbulence*, 1st edn. Cambridge University Press.

Fung, J. C. H., Hunt, J. C. R., Malik, N. A. & Perkins, R. J. 1992 Kinematic Simulation of homogeneous turbulence by unsteady random Fourier modes. *J. Fluid Mech.* **236**, 281–317.

Fung, J. C. H. & Vassilicos, J. C. 1998 Two-particle dispersion in turbulentlike flows. *Phys. Rev. E* **52**, 1677–1690.

Gargett, A. E., Osborn, T. R. & Nasmyth, P. W. 1984 Local isotropy and the decay of turbulence in a stratified fluid. *J. Fluid Mech* **144**, 231–280.

Godeferd, F. S. & Cambon, C. 1994 Detailed investigation of energy transfers in homogeneous stratified turbulence. *Phys. Fluids* **6**, 2084–2100.

Godeferd, F. S., Malik, N. A., Cambon, C. & Nicolleau, F. 1997 Eulerian and Lagrangian statistics in homogeneous stratified flows. *Appl. Sci. Res.* **57**, 319–335.

Hanazaki, H. & Hunt, J. C. R. 1996 Linear processes in unsteady stably stratified turbulence. *J. Fluid Mech.* **318**, 303–337.

Haren, L. van 1993 Étude théorique et modélisation de la turbulence en présence d'ondes internes. PhD thesis, École Centrale de Lyon.

Heppe, B. M. O. 1997 Stochastic models of dispersion and mixing in homogeneous turbulence. PhD thesis, University of Cambridge.

Kaneda, Y. & Ishida, T. 2000 Suppression of vertical diffusion in strongly stratified turbulence. *J. Fluid Mech.* **402**, 311–327.

Kimura, Y. & Herring, J. R. 1996 Diffusion in stably stratified turbulence. *J. Fluid Mech.* **328**, 253–269.

Malik, N. A. & Vassilicos, J. C. 1999 A Lagrangian model for turbulent dispersion with turbulent-like flow structure: comparison with DNS for two-particle statistics. *Phys. Fluids* **11**, 1572–1580.

Pearson, H. J. 1980 Disturbances and displacements in stratified fluids. PhD thesis, University of Cambridge.

Pearson, H. J., Puttock, J. S. & Hunt, J. C. R. 1983 A statistical model of fluid-element motions and vertical diffusion in a homogeneous stratified turbulent flow. *J. Fluid Mech.* **129**, 219–249.

Pedrizzetti, G. & Novikov, E. A. 1994 On Markov modelling of turbulence. *J. Fluid Mech.* **280**, 69–93.

Perry, A. E. & Chong, M. S. 1987 A study of eddying motions and flow patterns using critical point concepts. *Ann. Rev. Fluid Mech.* **19**, 125.

Tatarski, V. I. 1960 Radiophysical methods of investigating atmospheric turbulence. *Izv. Vyssh. Uchebn. Zaved. Radiofiz.* **4**, 551.

Taylor, G. I. 1921 Diffusion by continuous movements. *Proc. Lond. Math. Soc.* A **20**, 196.

Thomson, D. J. 1987 Criteria for selection of stochastic models of particle trajectories in turbulent flows. *J. Fluid Mech.* **180**, 529.

Vincent, A., Michaud, G. & Meneguzzi, M. 1996 On the turbulent transport of a passive scalar by anisotropic turbulence. *Phys. Fluids* **8**, 1312–1320.

Wray, A. A. & Hunt, J. C. R. 1990 Algorithms for classification of turbulent structures. In *IUTAM Symp. on Topological Fluid Mechanics* (ed. H. K. Moffat & A. Tsinober). Cambridge University Press.